High Temperature Electromechanical Response of Multilayer Piezoelectric Laminates under AC Electric Fields for Fuel Injector Applications

doi: 10.1007/s10999-019-09453-1

High Temperature Electromechanical Response of Multilayer Piezoelectric Laminates under AC Electric Fields for Fuel Injector Applications

Fumio Narita*, Ryohei Hasegawa and Yasuhide Shindo

Department of Materials Processing, Graduate School of Engineering, Tohoku University,

Aoba-yama 6-6-02, Sendai 980-8579, Japan

Abstract

This paper examines theoretically and experimentally the dynamic electromechanical response of multilayer piezoelectric laminates for fuel injectors at high temperatures. A phenomenological model of depolarization at high temperatures was used, and the temperature dependent piezoelectric coefficients were obtained. The high temperature electromechanical fields of the multilayer piezoelectric actuators under AC electric fields were then calculated by the finite element method. In addition, test data on the electric field induced strain at high temperatures, which verify the model, were presented.

*Corresponding author. Tel. & Fax: 8122-795-7342

E-mail address: narita@material.tohoku.ac.jp

1. Introduction

Multilayer PZT ceramics play an important role as active electronic elements in fuel injector applications [1, 2], and are under severe environment conditions in many cases. Recently, Senousy et al. [3] evaluated the thermo-electro-mechanical behavior of PZT actuators applied to fuel injectors over a temperature range of -30 °C to 80 °C. Senousy et al. [4] also investigated the heat generation in PZT actuators for fuel injectors at dynamic operating conditions. In the case under cryogenic environment, Shindo et al. investigated the electromechanical response of multilayer PZT ceramics under DC [5–7] and AC [6–8] electric fields from room to liquid hydrogen temperature (20 K) for hydrogen fuel injector applications. On the other hand, Sapsathiarn et al. [9] analyzed the thermo-piezoelectric performance of PZT actuators in a hydrogen environment.

It is known that at high temperatures, the piezoelectric activity of PZT ceramics disappears due to depolarization [10]. Recently, Narita et al. [11] proposed a simple phenomenological model of the depolarization at high temperatures to evaluate the temperature dependent piezoelectric coefficients, and analyzed the electromechanical response of multilayer PZT actuators under DC electric field from room to high temperatures. They also measured the electric field induced strain for the actuators, and made a comparison between calculations and measurements [7].

In this paper, we investigate the dynamic electromechanical response of multilayer piezoelectric actuators under AC electric fields at high temperatures. A phenomenological model of the depolarization at high temperatures was used to predict the temperature dependent piezoelectric coefficients, and a finite element analysis (FEA) was carried out to discuss the high temperature electromechanical fields of the actuators, using the predicted piezoelectric coefficients. The AC electric field induced strain at high temperatures was also measured, and the test results were compared with numerical values. This comparison indicates a good agreement between the predictions and test data, and so suggests our model is reasonable.

2. Analysis

2.1 Basic equations

Consider a piezoelectric material with no body force and free charge. The field equations in the Cartesian coordinates $x_i (i = 1, 2, 3)$ are given by

$$\sigma_{ji,j} = \rho u_{i,tt} \tag{1}$$

$$\varepsilon_{ijk} E_{k,j} = 0, D_{i,i} = 0 \tag{2}$$

where σ_{ij}, u_i, E_i, D_i are the components of the stress tensor, displacement vector, electric field intensity vector, electric displacement vector, respectively, ρ is the mass density, ε_{ijk} is the permutation symbol, a comma denotes partial differentiation with respect to the coordinates x_i or the time t, and the Einstein summation convention over repeated indices is used. The relation between the strain tensor component ε_{ij} and the displacement vector component u_i is given by

$$\varepsilon_{ij} = \frac{1}{2}(u_{j,i} + u_{i,j}) \tag{3}$$

and the electric field intensity vector component is

$$E_i = -\phi_{,i} \tag{4}$$

where ϕ is the electric potential. Constitutive relations can be written as

$$\varepsilon_{ij} = s_{ijkl}\sigma_{kl} + \bar{d}_{kij} E_k \tag{5}$$

$$D_i = \bar{d}_{ikl}\sigma_{kl} + \epsilon^T_{ik} E_k \tag{6}$$

where s_{ijkl}, $\bar{d}_{kij}$, ϵ^T_{ik} are the elastic compliance, temperature dependent direct piezoelectric coefficient, and permittivity at constant stress, respectively, which satisfy the following symmetry relations:

$$s_{ijkl} = s_{jikl} = s_{ijlk} = s_{klij}, \bar{d}_{kij} = \bar{d}_{kji}, \epsilon^T_{ik} = \epsilon^T_{ki} \tag{7}$$

The constitutive equations (5) and (6) for piezoelectric material poled in the x_3-direction are found in Appendix A.

2.2 Finite element method

We consider a multilayer piezoelectric laminate with many PZT layers of width W_p and thickness h_p, thin electrodes, and elastic coating layer of thickness h_e. In order to discuss the electromechanical fields near the internal electrode at room and high temperatures, the problem of the multilayer piezoelectric laminate is solved using the unit cell model. Fig. 1 shows the unit cell (2-layer piezoelectric laminate with $|x| \leq W_p/2 + h_e, |y| \leq W_p/2 + h_e, 0 \leq z \leq 2h_p$). A rectangular Cartesian coordinate system O-xyz is used and the origin of the coordinate system coincides with the center of the laminate. The x, y, z-axes coincide with the x_1, x_2, x_3-direction. Each PZT layer is sandwiched between alternating positive and negative thin electrodes of length a and width W_p, and the layers are electrically in parallel and mechanically in series. An electrically active $2a - W_p$ region exists in the portions of the laminate where the positive and negative electrodes overlap, while an electrically inactive $W_p - a$ tab region exists on both sides of the laminate. The poling directions of the upper and lower PZT layers are opposite so that the vertical displacement (z-direction) in adjacent layer can be accumulated. Due to the geometric and loading symmetry, only the half needs to be analyzed. The electrode layers are not incorporated into the model.

The PZT layers are made up of many grains. After poling, each PZT layer has an average polarization. Here, each grain is modeled as a uniformly polarized cell that contains a single domain, i.e., each grain is equivalent to a uniformly polarized single domain. The model neglects the interaction among different grains (domains). In reality, this is not true, but the assumption does not affect the macroscopic behavior of the multilayer piezoelectric laminates from room to high temperatures.

It is known that the operating temperatures have been limited to one half of Curie temperature, $T_c/2$, due to the depolarization. Here, it is assumed that when the temperature T increases from room temperatures (RT), the poling direction of each grain (domain) begins to rotate at $T_c/2$ and the rotation angle α becomes $\pi/2$ in the $\pm x$- or $\pm y$-direction at T_c. The angle $\alpha = 0$ from RT to $T_c/2$ corresponds to the direction of first poling axis (z-direction). Also assume that the piezoelectric properties decrease linearly as T increases from $T_c/2$ to T_c. For simplicity here, we assume that the elastic and dielectric properties of PZT layers remain unchanged after the depolarization occurs. The

temperature dependent direct piezoelectric coefficient in each grain (domain) is

$$\bar{d}_{ikl} = \left\{ d_{33} n_{\mathrm{P}i} n_{\mathrm{P}k} n_{\mathrm{P}l} + d_{31}(n_{\mathrm{P}i}\delta_{kl} - n_{\mathrm{P}i} n_{\mathrm{P}k} n_{\mathrm{P}l}) + \frac{1}{2} d_{15}(\delta_{ik} n_{\mathrm{P}l} - 2 n_{\mathrm{P}i} n_{\mathrm{P}k} n_{\mathrm{P}l} + \delta_{il} n_{\mathrm{P}k}) \right\} \quad (8)$$

where $n_{\mathrm{P}i}$ is the components of unit vector in the poling direction, δ_{ij} is the Kronecker delta, and d_{33}, d_{31} and d_{15} are the longitudinal, transverse and shear piezoelectric coefficients, respectively, when the PZT layers are completely poled.

We used a commercial finite package ANSYS, with eight-node SOLID5 element, to perform the analysis. A convergence study was conducted to establish the accuracy and validity of finite element results. The mesh size was varied until good convergence was obtained. The finite element mesh has 57,000 elements and 66,000 nodes. Each element is taken to represent a single grain (domain) of the PZT layer. Here, we define the rotation angle of poling in each element to be temperature dependent function $\alpha(T)$, and the unit vector in Eq. (8) is given by

$$\begin{aligned} n_{\mathrm{P}1} &= \sin\alpha(T)\cos\beta \\ n_{\mathrm{P}2} &= \sin\alpha(T)\sin\beta \\ n_{\mathrm{P}3} &= \cos\alpha(T) \end{aligned} \quad (9)$$

A random number generator is used to create the only angle β, with value of 0, $\pi/2$, π, or $3\pi/2$. The effective temperature dependent direct piezoelectric coefficient (donoted by superscript G) is related to the local direct piezoelectric coefficient $\bar{d}_{ijk}$ by

$$\bar{d}^{\mathrm{G}}_{ijk} = \frac{1}{2\pi}\int_0^{2\pi} \bar{d}_{ijk}\, d\beta \quad (10)$$

In the case under AC electric field at RT, we consider the extrinsic contribution due to domain wall motion [12]. Details can be found in Ref. 6. On the other hand, the domain wall motion becomes difficult to occer when the temperature is high, and we assume the piezoelectric behavior with no extrinsic contribution at high temperatures ($\geq T_{\mathrm{c}}/2$).

The electric potential on two electrode surfaces ($-W_p/2 \leq x \leq -W_p/2+a, 0 \leq y \leq W_p/2, z = 0, 2h_p$) equals the applied AC voltage, $\phi = V_0 \exp(i\omega t)$: V_0 is AC voltage amplitude and ω is angular frequency ($= 2\pi f$ where f is frequency in Hertz). The electrode surface ($W_p/2-a \leq x \leq W_p/2, 0 \leq$

$y \leq W_p/2, z = h_p$) is connected to the ground, so that $\phi = 0$. The mechanical boundary conditions include the traction-free conditions on the coating layer surfaces at $x = \pm(W_p/2+h_e), y = W_p/2+h_e$ and the symmetry conditions on the faces at $y = 0, z = 0, 2h_p$. In addition, the origin is constrained against the displacement in the x-direction, to avoid rigid body motion [13].

3. Experiments

Commercially supplied multilayer actuator using 300 soft PZT N-10 layers (NEC/Tokin Co. Ltd., Japan) of width W_p = 5.2 mm and thickness h_p = 0.1 mm was used. The material properties of N-10 at RT are listed in Table 1, and the coercive electric field is approximately E_c = 0.36 MV/m. The specimen and testing set up are shown in Fig. 2. A rectangular Cartesian coordinate system O-xyz is employed, and the origin of the coordinate system is located at the center of the actuator. The electrode length is $a = W_p$ = 5.2 mm (fully electrodes), and the PZT N-10 laminate is coated with epoxy layer of thickness h_e = 0.5 mm. The total dimensions of the actuator are width of 6.2 mm and length of 40.5 mm. The Curie temperature of N-10 is T_c = 145 °C. So, the temperature dependent rotation angle of the poling direction is assumed to be

$$\alpha(T) = \begin{cases} 0 & (25\,^\circ C \leq T \leq 73\,^\circ C) \\ (\pi/2)(1.38 \times 10^{-2} T - 1) & (73\,^\circ C \leq T \leq 145\,^\circ C) \end{cases} \tag{11}$$

Young's modulus, Poisson's ratio and mass density of epoxy layer are 3.35 GPa, 0.214 and 1100 kg/m^3, respectively.

The actuator was placed on the rigid body, and AC voltage at a frequency of f = 400 Hz was applied using an AC power supply. Two strain gages were attached at the center of the y = ±3.1 mm planes ($x = z = 0$ mm), and the magnitude of strain was measured. To control the temperature of the actuator, a constant temperature oven (DVS402, Yamato Scientific Co. Ltd., Japan) was used.

4. Results and discussion

We first present numerical and experimental results for the multilayer piezoelectric laminate with electrode length $a = W_p$ = 5.2 mm (fully electrodes). Fig. 3 shows the normal strain ε_{zz} versus electric field amplitude $E_0 = V_0/h_p$ at x = 0 mm, $y = W_p/2 + h_e$ = 3.1 mm and z = 0 mm of the laminate

at frequency f = 400 Hz and temperature T = 25 and 125 °C. The solid lines represent the strains of FEA with the domain wall motion effect. The open circle denotes the experimental data. It is shown that the strain of the laminate increases as the electric field amplitude increases. We see that the trend is sufficiently similar between the prediction and measurement, and the domain wall motion may not occur in the multilayer piezoelectric laminate under AC electric fields at 125 °C. At high temperatures, the poled piezoelectric crystal changes to a structure of cubic phase and the alignment of the dipoles is lost. So the AC electric field induced strain at 125 °C is smaller than that at 25 °C.

Next, the electromechanical fields of the multilayer piezoelectric laminates obtained from the FEA are discussed. Fig. 4 shows the distribution of the normal stress σ_{zz} as a function of x at y = 0 mm and z = 0.025 mm for the multilayer piezoelectric laminates with a = 5.0 mm (partially electrodes) and a = 5.2 mm (fully electrodes) under E_0 = 0.3 MV/m at f = 400 Hz and T = 125 °C. For the piezoelectric laminate with partially electrodes, a high normal stress occurs in the inactive region. It seems that the presence of electrode tip creates the most suitable stress conditions for the initiation of cracking. This situation may be applicable to the other multilayer piezoelectric laminates with different size and shape. The results for the evaluation of stresses in the multilayer piezoelectric laminates may help fuel injector designers to estimate the fracture risk and to optimize in-service loading conditions. Fig. 5 shows the distribution of the electric field E_z as a function of x at y = 0 mm and z = 0.025 mm for the multilayer piezoelectric laminates with a = 5.0 mm (partially electrodes) and a = 5.2 mm (fully electrodes) under E_0 = 0.3 MV/m at f = 400 Hz and T = 125 °C. For the piezoelectric laminate with partially electrodes, a high electric field is observed near the electrode tip (x = 2.4 mm). The results on the electric field distributions show that if the multilayer piezoelectric laminates with partially electrodes are applied to fuel injectors, the dielectric breakdown or electric fatigue is expected near the electrode tip, and the fuel injector designers need to be aware of electric field behavior.

5. Conclusions

This paper presents the results of numerical and experimental study on the dynamic electrome-

chanical response of multilayer piezoelectric laminates at high temperatures. We estimated the temperature dependent piezoelectric coefficients and showed that the calculated strain versus AC electric field curves at high temperatures are reasonably accurate, in agreement with measured data. It was found that the AC electric field induced stain decreases with increasing temperature due to the depolarization. It was also shown that the stress and electric field in the piezoelectric layers for the laminate with partially electrodes are very high near the electrode tip. This study may be useful in designing high performance fuel piezoelectric injectors.

References

[1] P. Glynne-Jones, M. Coletti, N. M. White, S. B. Gabrielm and C. Bramanti, 2010, “A Feasibility Study on Using Inkjet Technology, Micropumps, and MEMs as Fuel Injectors for Bipropellant Rocket Engines, ”Acta Astronaut., **67**, pp. 194-203.

[2] C. A. Satkoski, G. M. Shaver, R. More, P. Meckl, D. Memering, S. Venkataraman, J. Syed, and J. Carmona-Valdes, 2011, “Dynamic Modeling of a Piezoelectric Actuated Fuel Injector, ”J. Dyn. Sys., Meas., Control, **133**, p. 051011.

[3] M. S. Senousy, F. X. Li, D. Mumford, M. Gadala, and R. K. N. D. Rajapakse, 2009, “Thermo-electro-mechanical Performance of Piezoelectric Stack Actuators for Fuel Injector Applications, ”J. Intell. Mater. Syst. Struct., **20**, pp. 387-399.

[4] M. S. Senousy, R. K. N. D. Rajapakse, D. Mumford, and M. S. Gadala, 2009, “Self-heat generation in piezoelectric stack actuators used in fuel injectors, ”Smart Mater. Struct., **18**, p. 045008.

[5] Y. Shindo, F. Narita, and T. Sasakura, 2011, “Cryogenic Electromechanical Behavior of Multilayer Piezo-Actuators for Fuel Injector Applications, ”J. Appl. Phys., **110**, p. 084510.

[6] Y. Shindo and F. Narita, 2012, “Piezomechanics in PZT Stack Actuators for Cryogenic Fuel Injectors,” Smart Actuation and Sensing Systems - Recent Advances and Future Challenges, Rocco Vertechy and Gabriele Vassura (Eds.), InTech Publishing Company, pp. 639-656.

[7] Y. Shindo, 2015, “Dielectric/Ferroelectric Material Systems and Structures’, Electromagneto-Mechanics of Material Systems and Structures, Wiley, pp. 49-218.

[8] Y. Shindo, T. Sasakura, and F. Narita, 2012, “Dynamic Electromechanical Response of Multilayered Piezoelectric Composites from Room to Cryogenic Temperatures for Fuel Injector Applications, ”ASME J. Eng. Mater. Technol., **134**, p. 031007.

[9] Y. Sapsathiarn, Y. Singh, and R. K. N. D. Rajapakse, 2014, “Numerical Modelling of Piezo-electric Actuators Exposed to Hydrogen, ”Acta Mechanica, **225**, pp. 2943- 2957.

[10] R. C. Turner, P. A. Fuierer, R. E. Newnham, and T. R. Shrout, 1994, “Materials for High Temperature Acoustic and Vibration Sensors: A Review, ”Appl. Acoust., **41**, 299-324.

[11] F. Narita, R. Hasegawa, and Y. Shindo, 2014, “Electromechanical Response of Multilayer Piezoelectric Actuators for Fuel Injectors at High Temperatures, ”J. Appl. Phys., **110**, p. 084510.

[12] F. Narita, Y. Shindo, and M. Mikami, 2005, “Analytical and Experimental Study of Nonlinear Bending Response and Domain Wall Motion in Piezoelectric Laminated Actuators under AC Electric Fields, ”Acta Mater., **53**, pp. 4523-4529.

[13] C. L. Hom and N. Shankar, 1995, “A Numerical Analysis of Relaxor Ferroelectric Multilayered Actuators and 2-2 Composite Arrays, ”Smart Mater. Struct. **4**, pp. 305-317.

Appendix A

For piezoelectric ceramics which exhibit symmetry of a hexagonal crystal of class 6 mm with respect to principal x_1, x_2, and x_3 (poling) axes, the constitutive relations can be written in the following form:

$$\left\{\begin{array}{c}\varepsilon_{11}\\ \varepsilon_{22}\\ \varepsilon_{33}\\ 2\varepsilon_{23}\\ 2\varepsilon_{31}\\ 2\varepsilon_{12}\end{array}\right\} = \left[\begin{array}{cccccc} s_{11} & s_{12} & s_{13} & 0 & 0 & 0\\ s_{12} & s_{11} & s_{13} & 0 & 0 & 0\\ s_{13} & s_{13} & s_{33} & 0 & 0 & 0\\ 0 & 0 & 0 & s_{44} & 0 & 0\\ 0 & 0 & 0 & 0 & s_{44} & 0\\ 0 & 0 & 0 & 0 & 0 & s_{66}\end{array}\right]\left\{\begin{array}{c}\sigma_{11}\\ \sigma_{22}\\ \sigma_{33}\\ \sigma_{23}\\ \sigma_{31}\\ \sigma_{12}\end{array}\right\} - \left[\begin{array}{ccc} 0 & 0 & \bar{d}_{31}\\ 0 & 0 & \bar{d}_{31}\\ 0 & 0 & \bar{d}_{33}\\ 0 & \bar{d}_{15} & 0\\ \bar{d}_{15} & 0 & 0\\ 0 & 0 & 0\end{array}\right]\left\{\begin{array}{c}E_1\\ E_2\\ E_3\end{array}\right\} \tag{A.1}$$

$$\left\{\begin{array}{c}D_1\\ D_2\\ D_3\end{array}\right\} = \left[\begin{array}{cccccc} 0 & 0 & 0 & 0 & \bar{d}_{15} & 0\\ 0 & 0 & 0 & \bar{d}_{15} & 0 & 0\\ \bar{d}_{31} & \bar{d}_{31} & \bar{d}_{33} & 0 & 0 & 0\end{array}\right]\left\{\begin{array}{c}\sigma_{11}\\ \sigma_{22}\\ \sigma_{33}\\ \sigma_{23}\\ \sigma_{31}\\ \sigma_{12}\end{array}\right\} + \left[\begin{array}{ccc} \epsilon_{11}^{\mathrm{T}} & 0 & 0\\ 0 & \epsilon_{11}^{\mathrm{T}} & 0\\ 0 & 0 & \epsilon_{33}^{\mathrm{T}}\end{array}\right]\left\{\begin{array}{c}E_1\\ E_2\\ E_3\end{array}\right\} \tag{A.2}$$

where

$$\sigma_{23} = \sigma_{32}, \sigma_{31} = \sigma_{13}, \sigma_{12} = \sigma_{21} \;\Big\} \tag{A.3}$$

$$\varepsilon_{23} = \varepsilon_{32}, \varepsilon_{31} = \varepsilon_{13}, \varepsilon_{12} = \varepsilon_{21} \;\Big\} \tag{A.4}$$

$$\left.\begin{array}{l} s_{11} = s_{1111} = s_{2222},\ s_{12} = s_{1122},\ s_{13} = s_{1133} = s_{2233},\ s_{33} = s_{3333}\\ s_{44} = 4s_{2323} = 4s_{3131},\ s_{66} = 4s_{1212} = 2(s_{11} - s_{12})\end{array}\right\} \tag{A.5}$$

$$\bar{d}_{15} = 2\bar{d}_{131} = 2\bar{d}_{223},\ \ \bar{d}_{31} = \bar{d}_{311} = \bar{d}_{322},\ \ \bar{d}_{33} = \bar{d}_{333} \tag{A.6}$$

Table 1 Material properties of N-10

Elastic compliances					Piezoelectric coefficients			Permittivities		Mass density
s_{11}	s_{33}	s_{44}	s_{12}	s_{13}	d_{31}	d_{33}	d_{15}	ϵ_{11}^T	ϵ_{33}^T	ρ
($\times 10^{-12}\mathrm{m}^2/\mathrm{N}$)					($\times 10^{-12}\mathrm{m/V}$)			($\times 10^{-10}\mathrm{C/Vm}$)		($\mathrm{kg/m}^3$)
14.8	18.1	44.9	−5.1	−5.8	−287	635	930	443	481	8000

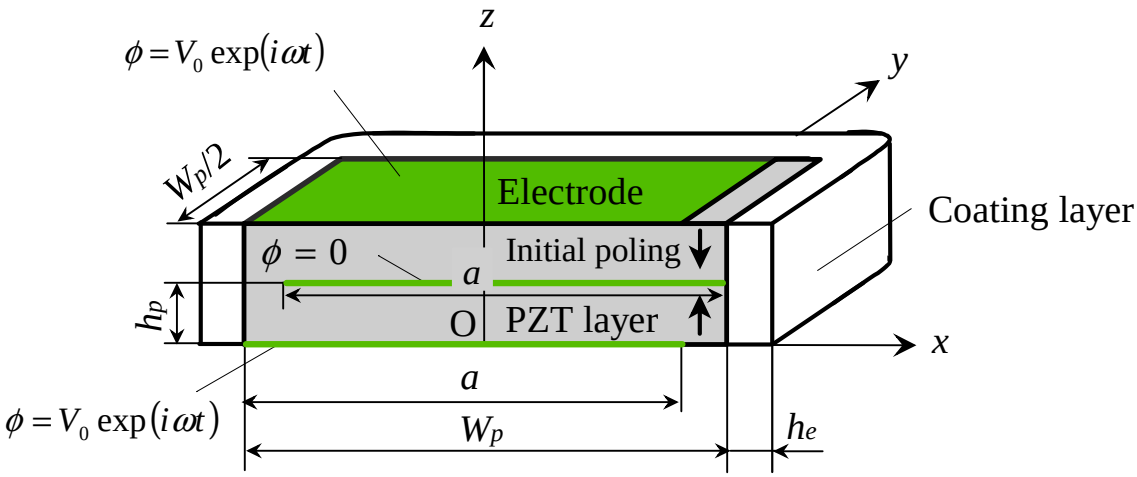

Fig. 1. Schematic diagram of finite element model

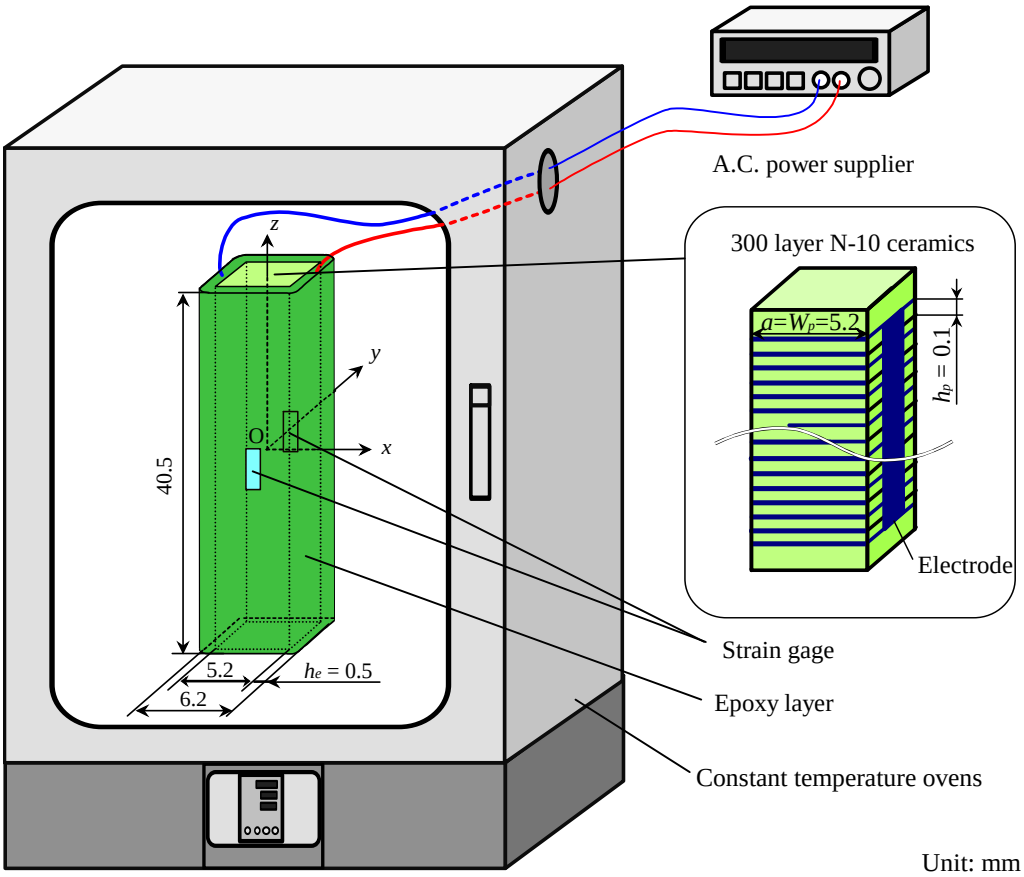

Fig 2. Experimental setup

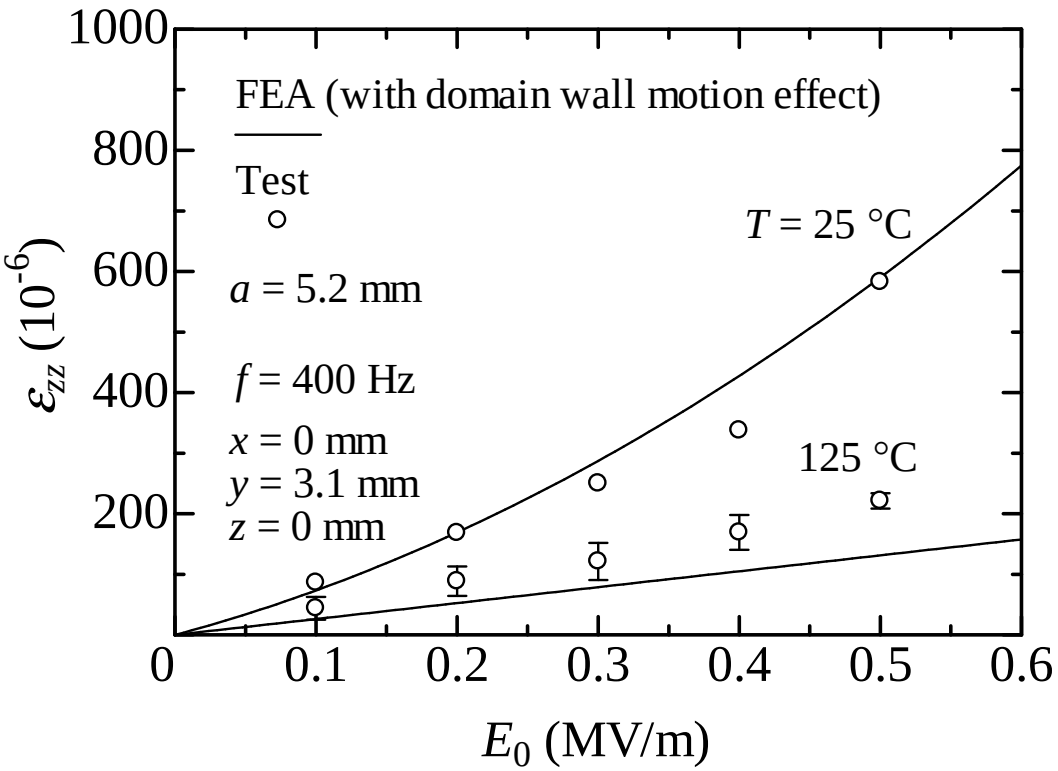

Fig 3. Normal strain versus electric field at x = 0 mm, y = 3.1 mm and z = 0 mm of piezoelectric actuator with fully electrodes

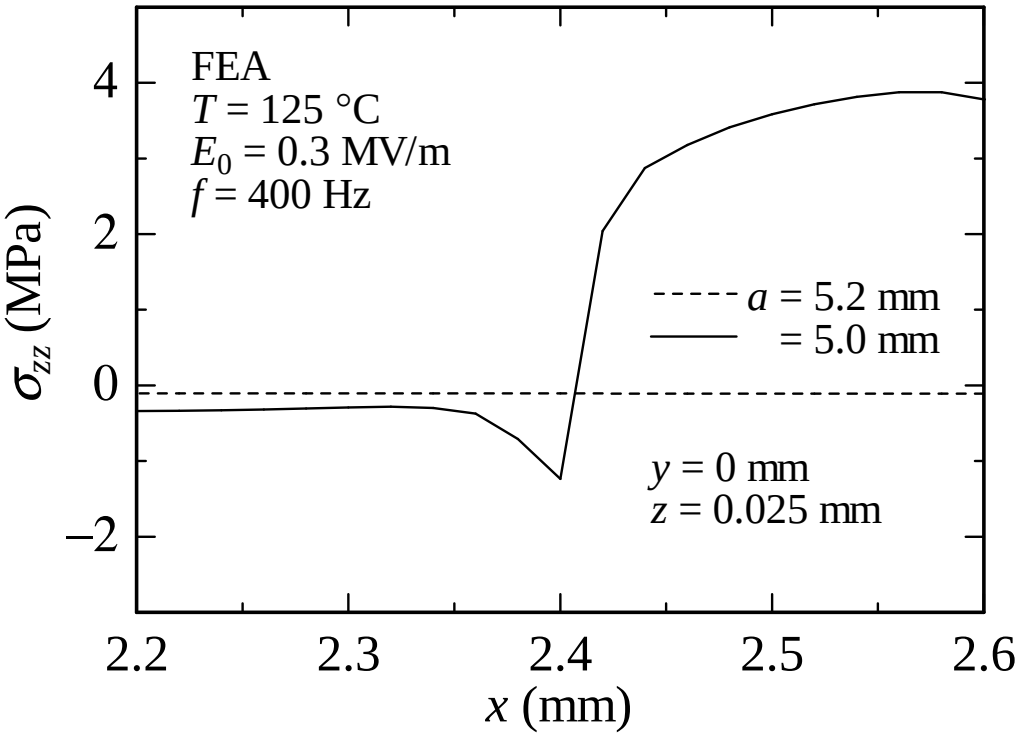

Fig 4. Variation of normal stress σ_{zz} as a function of x at y = 0 mm and z = 0.025 mm for piezoelectric actuators with fully and partially electrodes

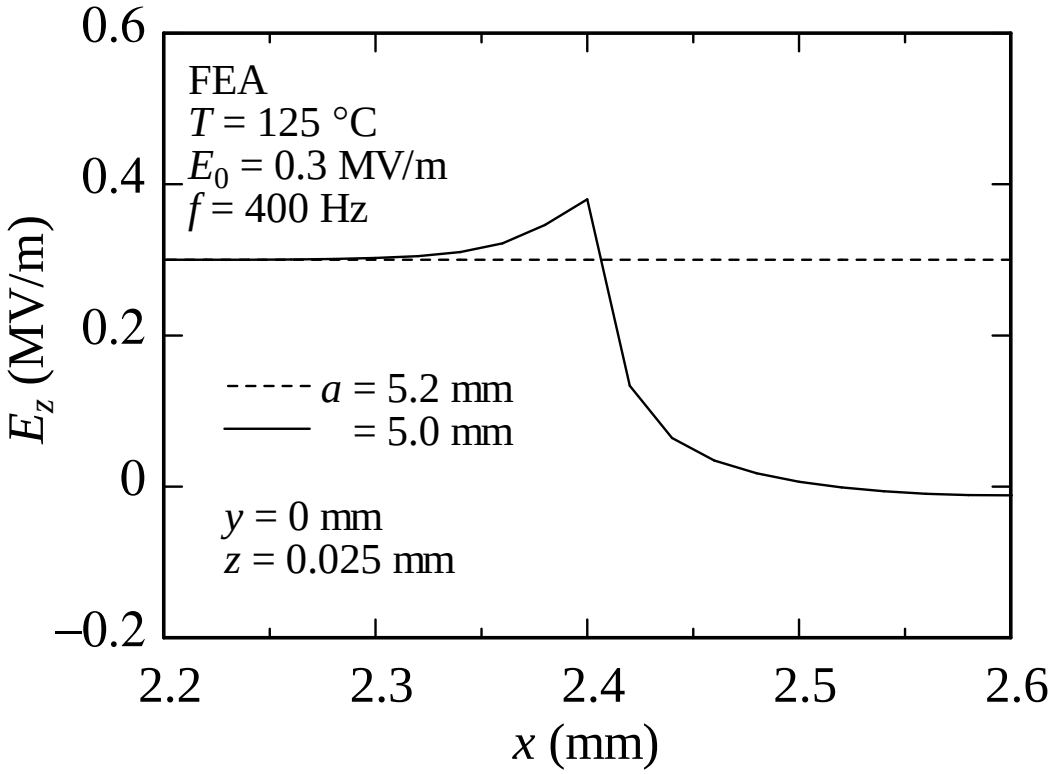

Fig 5. Variation of electric field E_z as a function of x at y = 0 mm and z = 0.025 mm for piezoelectric actuators with fully and partially electrodes